Identifying Soil Patterns at Different Spatial Scales with a Multi-Receiver EMI Sensor

Timothy Saey*
Philippe De Smedt
Dep. of Soil Management
Ghent Univ.
Coupure 653, 9000 Gent
Belgium

Wim De Clercq
Dep. of Archaeology
Ghent Univ.
Sint-Pietersnieuwstraat 35, 9000 Gent
Belgium

Eef Meerschman
Mohammad Monirul Islam
Marc Van Meirvenne
Dep. of Soil Management
Ghent Univ.
Coupure 653, 9000 Gent
Belgium

Multi-receiver electromagnetic induction (EMI) sensors are increasingly being used to map soil spatial variability by measuring the apparent electrical conductivity (ECa) of multiple soil volumes. We present a procedure to process such measurements to identify both large-scale soil variability patterns and small-scale features such as archaeological traces. A 2.6-ha arable field in Belgium was selected since aerial surveys indicated the presence of fine archaeological traces being masked partly by what appeared to be a trend in the soil composition. A survey with a DUALEM-21S EMI sensor provided four co-located ECa measurements of varying soil volumes, which were combined in a two-step inversion procedure. Our procedure enhanced the distinction between the archaeological traces and probable ice-wedge casts, with a small lateral and vertical extent, and the large-scale trend of natural soil variability, identified as the varying depth to the interface between two contrasting soil layers.

Abbreviations: DOE, depth of exploration; EC, electrical conductivity; ECa, apparent electrical conductivity; EMI, electromagnetic induction; LIN, low induction number; MEE, mean estimation error; RMSEE, root mean squared estimation error.

To investigate the soil constitution over shallower depths, EMI soil sensors have proved their functioning. These measure the ECa, which is primarily related to soil salinity (Heilig et al., 2011), and in nonsaline soils to several soil physical properties, such as moisture content and particle-size distribution: wetter soil is more electrically conductive than drier soil and coarser soil tends to be less so than finer soil (Carroll and Oliver, 2005; Inman et al., 2002). This makes multiple ECa measurements appropriate to determine the vertical distribution of soil electrical conductivity (EC). For the quantification of vertical differences in EC from aboveground ECa measurements, empirical relations were established (Rhoades et al., 1989). Rhoades and Corwin (1981) and Slavich (1990) used multiple linear regression to correlate ECa measurements to measured EC-profiles. The obtained coefficients were used to model EC-profiles at locations were EC-measurements were unavailable. Unfortunately, these coefficients are site-specific. McNeill (1980) presented a linear model of the EMI conductivity depth response. This approach is based on the fact that the response of ground conductivity meters at low conductivities is roughly a linear function of the EC at different depths. Corwin and Rhoades (1982) used these depth response functions to determine the EC of various depth intervals by developing linear combinations of the measurements from different coil orientations. The coefficients are selected to maximize the response of the instrument to EC in the region of interest. Cook and Walker (1992) improved this method by using optimization techniques to select coefficients that are, in a sense, optimal. Borchers et al. (1997) employed measure-

Soil Sci. Soc. Am. J. 77:382–390
doi:10.2136/sssaj2012.0276
Received 28 Aug. 2012
*Corresponding author (Timothy.Saey@UGent.be).

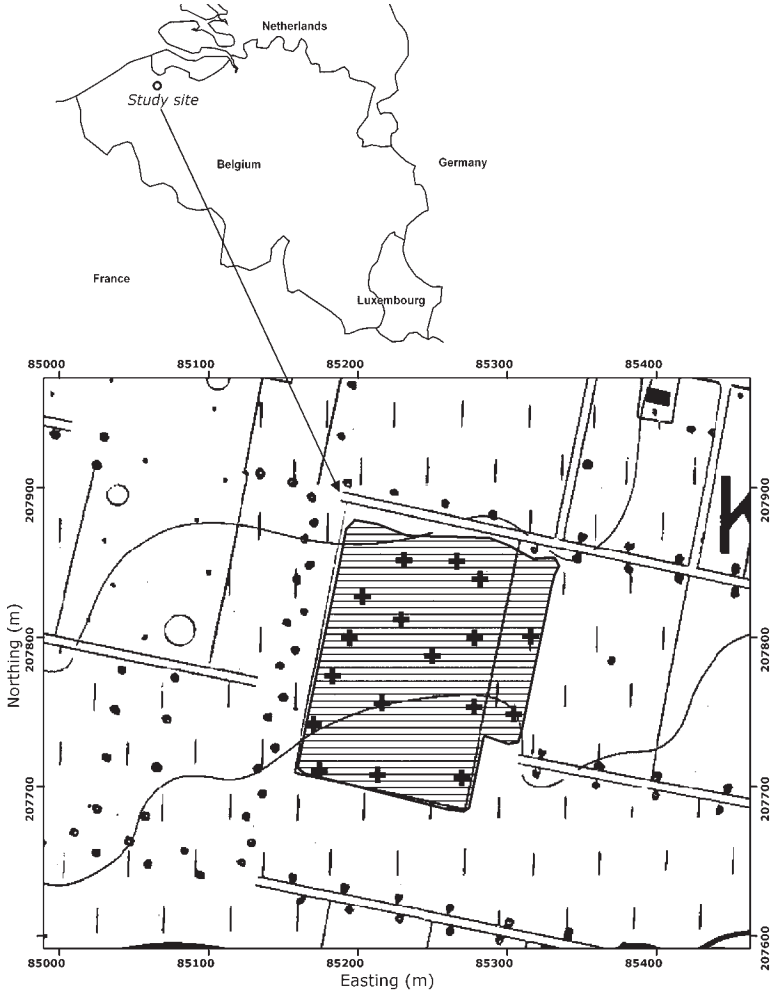

Fig. 1. Localization of the study site in Belgium and delineation on the topographic map with 17 validation points (cross symbols).

ments obtained at different heights above the soil surface that can be used to predict the electrical EC at different depths. They used the linear model of conductivity depth response with second order Tikhonov regularization because they expected soil EC profiles to vary in a smooth way.

Today, multi-receiver EMI instruments are increasingly being employed to obtain information about the EC over multiple soil volumes. Multi-receiver instruments offer significant benefits in extracting quantitative information about subsoil features (Saey et al., 2009a; Tromp-van Meerveld and McDonnell, 2009; Mester et al., 2011). Different depth responses are obtained for different coil orientations, different coil spacings, and different frequencies, which can be used for a multi-layer inversion (Saey et al., 2012a, 2012b).

With multi-receiver EMI instruments operating at a fixed frequency, increasing the coil spacing results in a deeper depth of exploration (DOE) and in a coarser signal resolution. Apart from the coil spacing, the coil orientation influences the depth sensitivity profile. Although the different coil configurations of multi-receiver instruments have different depth response functions, practice has shown that the resulting measurements are often quite similar (Saey et al., 2009a). A highly conductive soil layer, such as a clay substrate, has a substantial contribution to all ECa measurements, even if the layer is situated below the DOE of a particular coil configuration. Therefore, all measurements are influenced by this highly conductive layer. However, smaller conductive features within the subsurface can be difficult to discern as they can be masked by these highly contrasting layers deeper in the profile. Therefore, combining simultaneous measurements obtained from different EMI coil configurations with different depth sensitivity profiles enables information to be extracted about both the smaller conductive features in the subsurface and any underlying thick conductive layer. Several inversion procedures have been developed to integrate simultaneous sensor measurements. Monteiro Santos et al. (2010) inverted ECa data of multiple coil configurations based on a one-dimensional laterally constrained inversion algorithm to quantify the EC within a soil profile. Mester et al. (2011) developed a two-layer inversion algorithm using the different sensing depths of multi-configuration ECa data, minimizing the bias between the measured and modeled magnetic field. Saey et al. (2012a) inverted multiple ECa measurements to account for the conductivities within distinct depth intervals, while Saey et al. (2012b) modeled the depths of the interfaces between three distinct soil layers. These inversion procedures quantified the variability of soil conductivity within distinct, fixed depth intervals. However, they are unable to take into account the varying interface depth between strongly contrasting soil layers. Therefore, the objective of this study was to develop an inversion procedure to improve the identification of both small-scale archaeological features and the large-scale soil variability within varying depth intervals based on ECa data obtained with a multi-receiver EMI sensor. For this, we choose the inversion procedure of Saey et al. (2012a) as a basis.

MATERIALS AND METHODS

Study Area

Our study area is situated in the northwestern part of Belgium (Fig. 1). It is a 2.6-ha arable field located on a gentle hillside with an elevation ranging between 12.4 and 14.3 m above sea level. It has the central coordinates: 50°10′35″N lat, 3°26′35″E long.

The field is part of the "Maldegemvelt," a large area of poor wasteland situated between Ghent and Bruges, which was already partly cultivated during Roman and Medieval times. But it wasn't until the 18th century that the area was entirely converted to agricultural land use. Traces of buried constructions and anthropogenic activities were first discovered within our study field during an aerial photographic survey in 1987. A systematic follow-up of the site resulted in a dataset of 205 aerial images taken

under varying conditions. These images reveal several enclosures, ditches and possible pits, and wells, which are believed to originate from Roman and Medieval times (De Clercq et al., 2012).

On the national soil map the soil of this field is uniformly identified as a Carbic Podzol (WRB) or Humod according to the U.S. Soil Taxonomy without a contrasting substrate within 1.2 m of the soil surface. The soil developed in aeolian sand deposited during the Weichselian glacial stage. These sand deposits rarely reach a thickness of more than 1.2 m and are usually only a few decimeters thick. Sometimes they are even fully integrated into the plow layer (reaching a depth of 0.30–0.35 m). Below these deposits there exists a thick layer of marine clay from the Late Eocene.

Across the study site, a few soil samples were taken from the sand and the clay substrate and analyzed for their textural composition according to the conventional sieve-pipette method. The mean clay-silt-sand fractions (with boundaries 2-50-2000 μm, respectively) were determined. On average, the sandy topsoil has a much higher sand content (78.9%) and a much lower clay content (6.8%) than the clayey subsoil (7.8% sand and 65.4% clay).

The clay's depth below the surface must have had important consequences on the occupational history of the area because it causes the formation of a perched water table during wet seasons, which is unfavorable for growing agricultural crops (Ameryckx, 1962). Settlements most likely developed in areas with better drainage conditions, thus at locations with a thick sandy layer. These specific geological conditions probably influenced both the location and morphology of the existing settlements. Moreover, they contributed to an increased visibility during aerial and EMI survey.

Multi-Receiver EMI Sensor

In its simplest configuration, an EMI soil sensor consists of two coils separated by a fixed distance. A primary magnetic field (H_p) is created by the transmitting coil carrying a time-varying electric current at a set frequency. This field creates eddy currents in the soil below, which induce their own magnetic field (H_i). Both the induced secondary field and the primary field are recorded by the receiving coil at a fixed distance from the transmitter coil (McNeill, 1980). The ratio of the H_i to the H_p is recorded as in-phase and quadrature-phase data. From the quadrature data, the ECa of the bulk soil can be obtained, as a depth averaged conductivity value of the soil volume in mS m^{-1}. We used the DUALEM-21S instrument (DUALEM, Milton, Canada). Our EMI sensor was pulled in a nonmetal sled by an all-terrain vehicle at a speed of about 5 to 8 km h^{-1}, crossing the field at parallel lines spaced 0.75 m. Within the lines, measurement intervals were at approximately 0.25 m. The DUALEM-21S sensor consists of one transmitter coil and four receiver coils located at spacings of 1, 1.1, 2, and 2.1 m (Saey et al., 2009a). The 1- and 2-m transmitter-receiver pairs form a vertical dipole mode (HCP,1 and HCP,2), while the 1.1- and 2.1-m pairs form a perpendicular dipole mode (PRP,1.1 and PRP,2.1). Both transmitter-receiver spacing and orientation determine the depth and weighting response pattern of the signal. The cumulative response (expressed as a percentage of the measured signal, relative to 1) from the soil volume above a depth z (in m) was given by McNeill (1980) for the vertical [$R_{HCP}(z)$] dipole mode and by Wait (1962) for the perpendicular [$R_{PRP}(z)$] dipole mode:

$$R_{HCP}(z)=1-\left(4\frac{z^2}{s^2}+1\right)^{-0.5} \quad [1]$$

$$R_{PRP}(z)=2\frac{z^2}{s^2}\left(4\frac{z^2}{s^2}+1\right)^{-0.5} \quad [2]$$

with s being the transmitter-receiver spacing in m.

Consequently, DOE (or the depth at the 70% cumulative response) values are 0.5, 1.0, 1.5, and 3.2 m for the PRP,1.1; PRP,2.1; HCP,1; and HCP,2 coil configurations, respectively (Saey et al., 2009a).

The cumulative response functions are based on the assumption that the induction number (β) is very small [low induction number (LIN) conditions]. This is equivalent to stating that the current that flows in any loop of the magnetic field is completely independent of the current that flows in any other loop since they are not magnetically coupled (McNeill, 1980). Within the restriction of a small β, the McNeill approximation (1980) holds, which means that the instrument output is proportional to the ECa, and the depth response functions are independent of ECa (Hendrickx et al., 2002). However, Callegary et al. (2007) proved with numerical models based on Maxwell's equations that the depth response can be altered by soil properties affecting the ECa. Especially under high electrically conductive conditions, the simulated depth response function nonlinearly deviates from the function predicted from the McNeill (1980) approximation. It should also be noted that multi-receiver instruments, although intended to remain within the LIN condition, will intrinsically provide a progressive departure from the LIN condition with increasing coil separation and will potentially return different ECa values. These differences are not necessarily connected with "the variation of the conductivity with depth" and could better be regarded as a "geometrical" effect of the EMI measurement system (Beamish, 2011).

RESULTS

ECa Survey

Table 1 gives the summary statistics for the four data sets from each coil spacing. A total of 152,111 ECa data points were collected for each depth interval. As expected, the mean values

Table 1. Descriptive statistics (*m*: mean, *s*: standard deviation) of $ECa_{PRP,1.1}$, $ECa_{PRP,2.1}$, $ECa_{HCP,1}$ and $ECa_{HCP,2}$ for the study site (152,111 measurement points).

Variable	*m*	min	max	*s*
	mS m^{-1}			
$ECa_{PRP,1.1}$	19	6	78	7
$ECa_{PRP,2.1}$	45	24	91	12
$ECa_{HCP,1}$	57	30	98	12
$ECa_{HCP,2}$	89	65	130	13

increase with increasing DOE, indicating the deeper material to be more conductive than the topsoil. Also, the standard deviations increase with increasing DOE, which implies a higher variability at increased depths below the soil surface.

Ordinary kriging was used to interpolate the measurements to a 0.1- by 0.1-m grid. A maximum of 64 neighbors was used within a circular search area around the location being interpolated. Figure 2 shows the resulting ECa maps of the study area with a common legend scale for comparative reasons. The overall pattern of the four ECa maps is similar, i.e., a central north–south oriented band of lower values with higher values toward the eastern and western borders. The two PRP coil configurations (Fig. 2a and 2b) reveal linear features, which correspond to some of the features visible on the aerial photographs having an archaeological relevance as ditches forming part of an enclosure system (De Clercq et al., 2012). For all coil configurations, the highest values were found at the borders of the study site and the lowest in the center of the field. This large-scale pattern of soil variability tends to mask the smaller anthropogenic features, especially in the measurements with a deeper DOE.

For this reason, the deepest ECa measurements (1 and 2 m HCP) were used for modeling the depth-to-clay with a two-layered soil model following Saey et al. (2012b). Afterward, the shallow PRP data were used in a depth inversion procedure where the modeled paleotopography was taken into account to better visualize the small anthropogenic features while minimizing the effect of the large-scale soil variability.

Depth modeling

The inversion started with a fitting procedure to model the ECa values of both topsoil sandy (EC_{sand}) and subsoil clayey (EC_{clay}) layers by equating the modeled depths-to-clay from the HCP,1 ($z^{*}_{HCP,1}$) and HCP,2 coil configurations ($z^{*}_{HCP,2}$) (Saey et al., 2008). In a two-layered soil buildup, multiplying the relative weight with the EC of each layer and adding up all the layers results in the total $ECa_{HCP,s}$ of the investigated medium:

$$ECa_{HCP,1} = [R_{HCP,1}(z^{*}_{HCP,1}) - R_{HCP,1}(z_s)]EC_{sand} + [1 - R_{HCP,1}(z^{*}_{HCP,1})]EC_{clay} \quad [3]$$

$$ECa_{HCP,2} = [R_{HCP,2}(z^{*}_{HCP,2}) - R_{HCP,2}(z_s)]EC_{sand} + [1 - R_{HCP,2}(z^{*}_{HCP,2})]EC_{clay} \quad [4]$$

with z_s the height of the sensor above the soil (0.16 m). $R_{HCP,s}(z)$ is the cumulative response function above depth z of vertical coil configurations with intercoil spacing s (Eq. [1]). The cumulative responses from the sandy and clayey layers are $[R_{HCP,s}(z_{HCP,s}) - R_{HCP,s}(z_s)]$ and $[1 - R_{HCP,s}(z_{HCP,s})]$, respectively. The un-

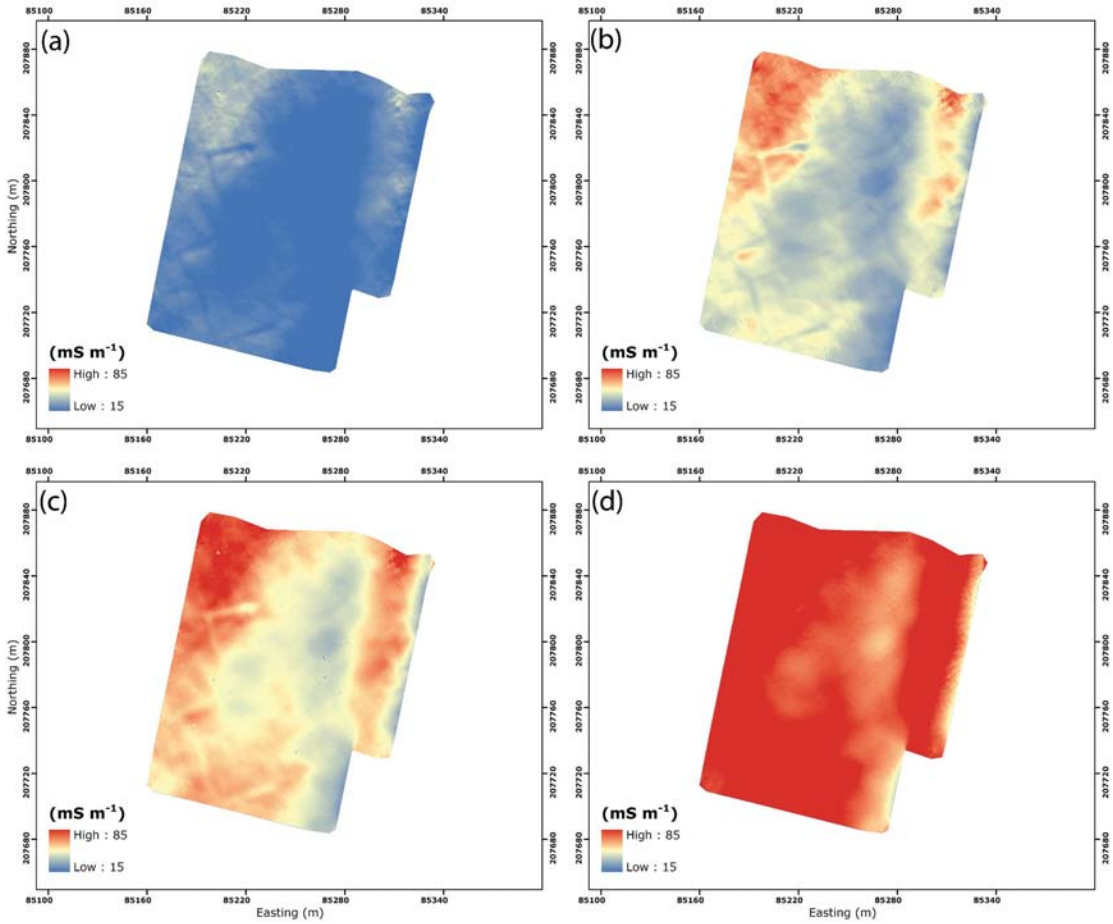

Fig. 2. ECa measurements for the coil configurations (a) PRP,1.1, (b) PRP,2.1, (c) HCP,1, and (d) HCP,2.

known and fixed parameters will be empirically determined by fitting $z^*_{HCP,1}$ to $z^*_{HCP,2}$.

Based on Eq. [3] and [4], $z^*_{HCP,1}$ to $z^*_{HCP,2}$ can be modeled given the $ECa_{HCP,s}$ measurements. Therefore, $R_{HCP,s}(z^*_{HCP,s})$ was calculated given the ECa measurements and the conductivities of both layers (EC_{sand} and EC_{clay}):

$$R_{HCP,s}(z^*_{HCP,s}) = \frac{ECa_{HCP,s} + [R_{HCP,s}(z_s)]EC_{sand} - EC_{clay}}{EC_{sand} - EC_{clay}} \quad [5]$$

These calculated $R_{HCP,s}(z^*_{HCP,s})$ can be put into Eq. [1] to obtain the modeled $z^*_{HCP,1}$ and $z^*_{HCP,2}$:

$$z^*_{HCP,s} = s\left(\frac{1}{4\cdot[1-R_{HCP,s}(z^*_{HCP,s})]^2} - 0.25\right)^{0.5} - z_s \quad [6]$$

To obtain the model parameters EC_{sand} and EC_{clay}, the sum of the squared differences between $z^*_{HCP,1}$ and $z^*_{HCP,2}$ was minimized for all 152,111 measurement locations:

$$\sum_{i=1}^{n}\left[z^*_{HCP,2}(i) - z^*_{HCP,1}(i)\right]^2 = \min \quad [7]$$

with i the number of the ECa measurement and n the total amount of measurements

The parameters EC_{sand} and EC_{clay} were iteratively adjusted to obtain the smallest sum of the squared differences between $z^*_{HCP,1}$ and $z^*_{HCP,2}$. It was found that $z^*_{HCP,1}$ and $z^*_{HCP,2}$ were very well fitted [mean estimation error (MEE) = 0.00 m, root mean squared estimation error (RMSEE) = 0.06 m and correlation (r) = 0.98]. The resulting parameters EC_{sand} and EC_{clay} were 7 and 133 mS m^{-1}.

Next, we modeled $z^*_{HCP,s}$ at each of the 152,111 measurement locations for both the 1 and 2 m HCP coil configurations given the fitted EC_{sand} and EC_{clay}:

$$ECa_{HCP,1} = [R_{HCP,1}(z^*_{HCP,s}) - R_{HCP,1}(z_s)]EC_{sand} + [1 - R_{HCP,1}(z^*_{HCP,s})]EC_{clay} \quad [8]$$

$$ECa_{HCP,2} = [R_{HCP,2}(z^*_{HCP,s}) - R_{HCP,2}(z_s)]EC_{sand} + [1 - R_{HCP,2}(z^*_{HCP,s})]EC_{clay} \quad [9]$$

This system was solved in Matlab using the Levenberg–Marquardt algorithm (Marquardt, 1963).

Validation of the Depth-to-Clay Model

The locations of 17 soil auger observations of the depth to the sand-clay interface were selected based on the HCP measurements of ECa and the x and y coordinates in such a way that their full range was covered (Fig. 1). This was done employing the conditioned Latin hypercube sampling approach (Minasny and McBratney, 2006). At all auger locations, we encountered the Eocene clay within 1.5 m from the surface. The average depth-to-clay was 1.05 ± 0.35 m. A comparison of the observed $z_{HCP,s}$ with the modeled $z^*_{HCP,s}$ is given in Fig. 3. The validation indices indicated a very good prediction: MEE = -0.02 m, RMSEE = 0.12 m, and r = 0.94. Therefore, we concluded that the modeled relationship had a low bias, a high accuracy, and the modeled depths correlated very well with the observed depths.

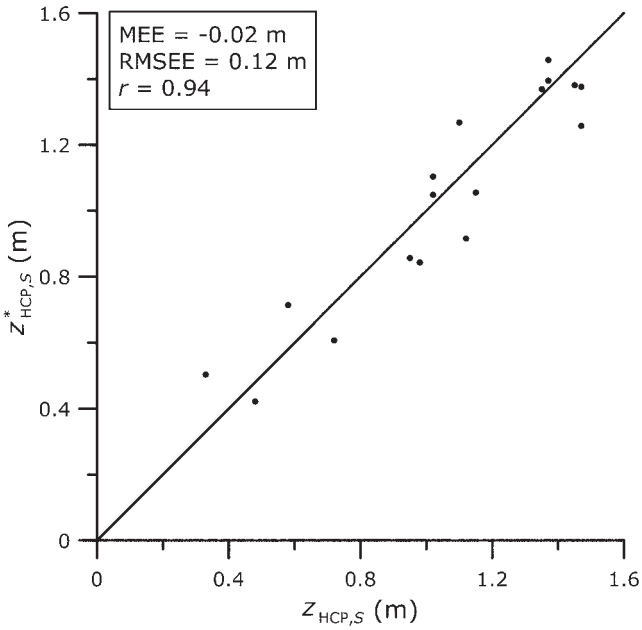

Fig. 3. Observed ($z_{HCP,s}$) versus modeled ($z^*_{HCP,s}$) depth-to-clay.

Reconstruction of the Sand-Clay Interface

The elevation of the study field (Z) and of the sand-clay interface are visualized in Fig. 4a and 4b, respectively. It can be observed that the Eocene clay sediments form a depression in the northern and central parts of the field. This depression was filled up with a 1.5 m thick aeolian sand layer. The depth of the sand-clay interface within this field is given in Fig. 4c together with the contour lines of 0.8 and 1.20 m. The latter could be used to upgrade the Belgian soil map as Vitharana et al. (2008) did.

Modeling the EC_{sand} across the Study Site

Given the modeled $z^*_{HCP,s}$ at each measurements location, the ECa measurements from the PRP coil configurations were filtered to extract the effect of the varying depth-to-clay, aiming at enhancing the small-scale features with faint ECa contrasts within the sandy layer. Therefore, an inversion procedure was applied, involving both PRP coil configurations, the EC_{clay} (constant across the study site) and the modeled $z^*_{HCP,s}$.

The two-layered depth model allowed inverting the simultaneous ECa measurements in the PRP coil configuration to obtain the conductivity of the sandy substrate (EC^*_{sand}), given the fixed EC_{clay} (133 mS m^{-1}) and the $z^*_{HCP,s}$, variable across the study site.

Therefore, the following set of equations was developed:

$$ECa_{PRP,s} = [R_{PRP,s}(z_{HCP,s} + z_s) - R_{PRP,s}(z_s)]EC^*_{sand} + [1 - R_{PRP,s}(z_{HCP,s} + z_s)]EC_{clay} \quad [10]$$

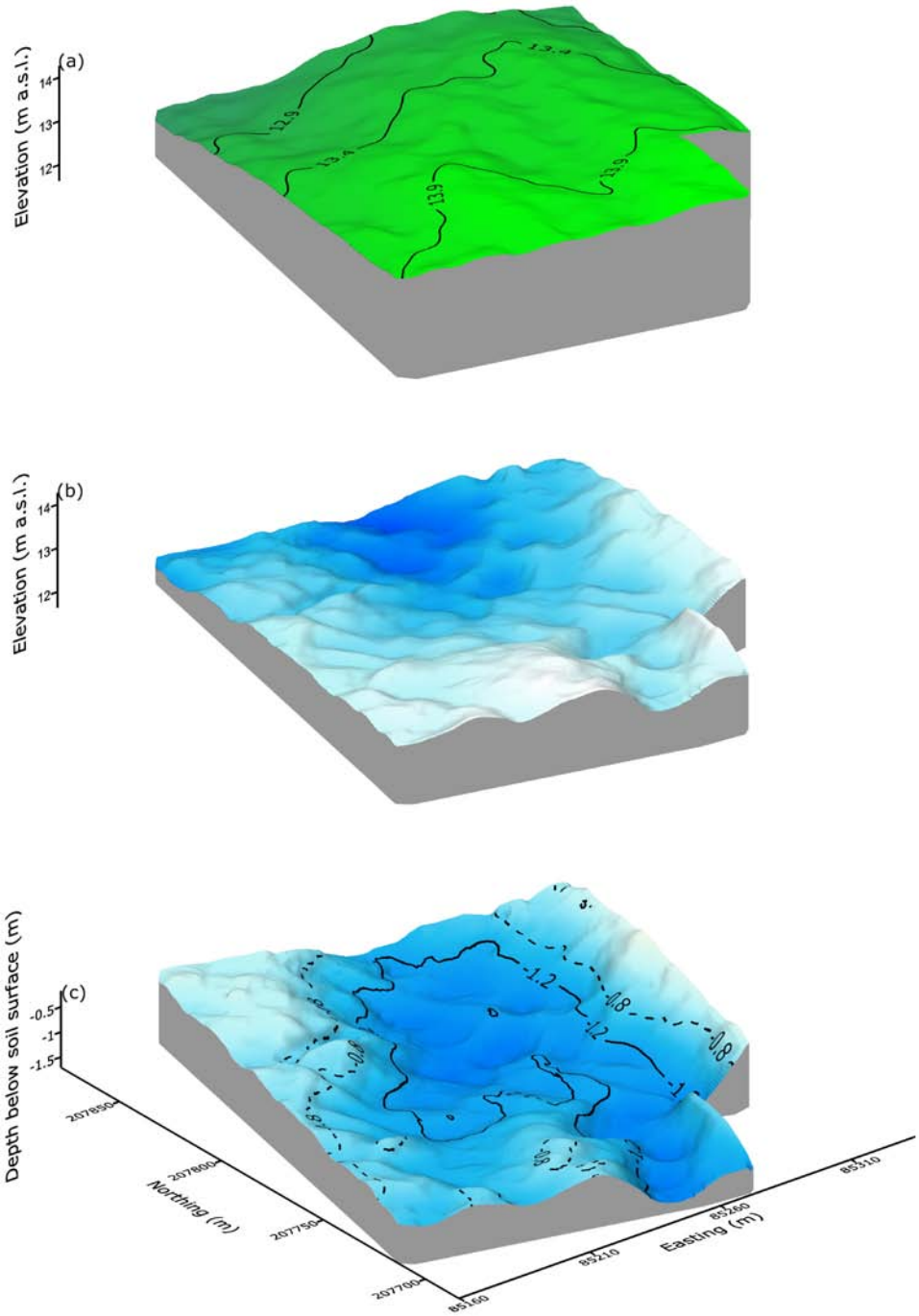

Fig. 4. Elevation of the current soil surface of the (a) study area and of the (b) modeled top of the Eocene clay. (c) shows the depth of the sand-clay interface ($z^{*}_{HCP,s}$) with indication of the 0.80- and 1.20-m depth contours.

with $R_{PRP,s}(z)$ being the cumulative responses above a depth z for the PRP configuration and coil spacing s (either 1.1 or 2.1 m). At each of the 152,111 measurement locations, the nonlinear Eq. [10] for both the 1.1 and 2.1 m coil configurations were combined to model the unknown EC^{*}_{sand}. This system was also solved using the Levenberg–Marquardt algorithm.

For comparative reasons Fig. 5 shows again the map of $ECa_{PRP,1.1}$ (the same data as Fig. 2a but using a different legend scale) and a map of the modeled EC^{*}_{sand}. The modeled EC^{*}_{sand} map shows more clearly the anthropogenic small-scale features and, in addition, new features become apparent. In the northeastern and western part of the study site, probable ice-wedge casts, being remnants of thermal contraction cracks formed under permafrost conditions during the Pleistocene glacial periods (Meerschman et al., 2011) appear as distinct hexagonal patterns.

Evaluating the Inversion Procedure

As an evaluation of the presented inversion procedure, a second inversion procedure was conducted as proposed by Saey et al. (2012a). Hereby, the EC was modeled within predefined depth intervals: 0 to 0.5 m (EC^{*}_{1}), 0.5 to 1.0 m (EC^{*}_{2}), and deeper than 1.0 m (EC^{*}_{3}), without taking the depth-to-clay into account (Fig. 6). Although these modeled EC maps allow a better interpretation of the small features than the unprocessed data, (Fig. 5a), the influence from the underlying clay layer remains present. Furthermore, unrealistic conductivity values were obtained. When the depth-to-clay is taken into account as in Fig. 5b, this interference is greatly reduced, allowing a more straightforward discrimination of the small-scale variation in the field.

DISCUSSION

Several studies employed the ECa from the EM38 and EM31 instruments to identify archaeological features. Fröhlich Gugler and Gex (1996) have found that ECa measurements are particularly suited for locating refills of ditches and trenches. Venter et al. (2006) identified basalt features and stone foundations from ECa anomalies. Persson and Olofsson (2004) found a former excavation tunnel in their ECa measurements, while Lück et al. (2003) identified small structures such as posts or pits and larger ditch systems. Santos et al. (2009) enhanced the conductivity response from archaeological targets that were not clearly distinguished due to variations in topography. These topographic effects in the ECa data are associated with variations in underground conductivity, caused by conductive sediment layers and the water table depth that follows the topography.

In general, ECa techniques prove to be an effective tool for mapping both the large- and small-scale soil variability but are governed by the status of the soil water content at the time of the ECa mapping. Brevik et al. (2006) proved that soil water content exerts a significant influence on the soil ECa. However, the relationship between ECa and the soil textural composition is more stable at higher water contents, implying that ECa mapping should be conducted under wet (near field capacity) soil conditions (McCutcheon et al., 2006). Therefore, ECa measurements were taken when a near to field capacity moisture tension was observed at the study site. In these conditions, strong deviations in ECa are likely to indicate a variation in soil textural composition (Saey et al., 2009b; Robinson et al., 2012). In situations where a textural discontinuity exists between two homogeneous layers, the spatial variability in ECa can be attributed to differences in depth of the interface between both layers (Doolittle et al., 1994).

Having revealed the build-up of the site, it became possible to explain why some fine-scale features were only faintly detected in the ECa measurements within some parts and clearly visible in other parts of the field. At locations where the clay substrate is shallow, the contrast with the anthropogenic features, which were filled-in with low-conductive sandy material, is very distinct. In the central part of the field, the anthropogenic features were dug entirely in the deeper sandy deposits, and hence, their contrast was much fainter.

After removing the effect of the variable depth-to-clay by integrating the multi-receiver EMI measurements, the discrimination between the small-scale features and the surrounding soil was enhanced, facilitating the recognition of both the archaeological features and probable ice-wedge casts.

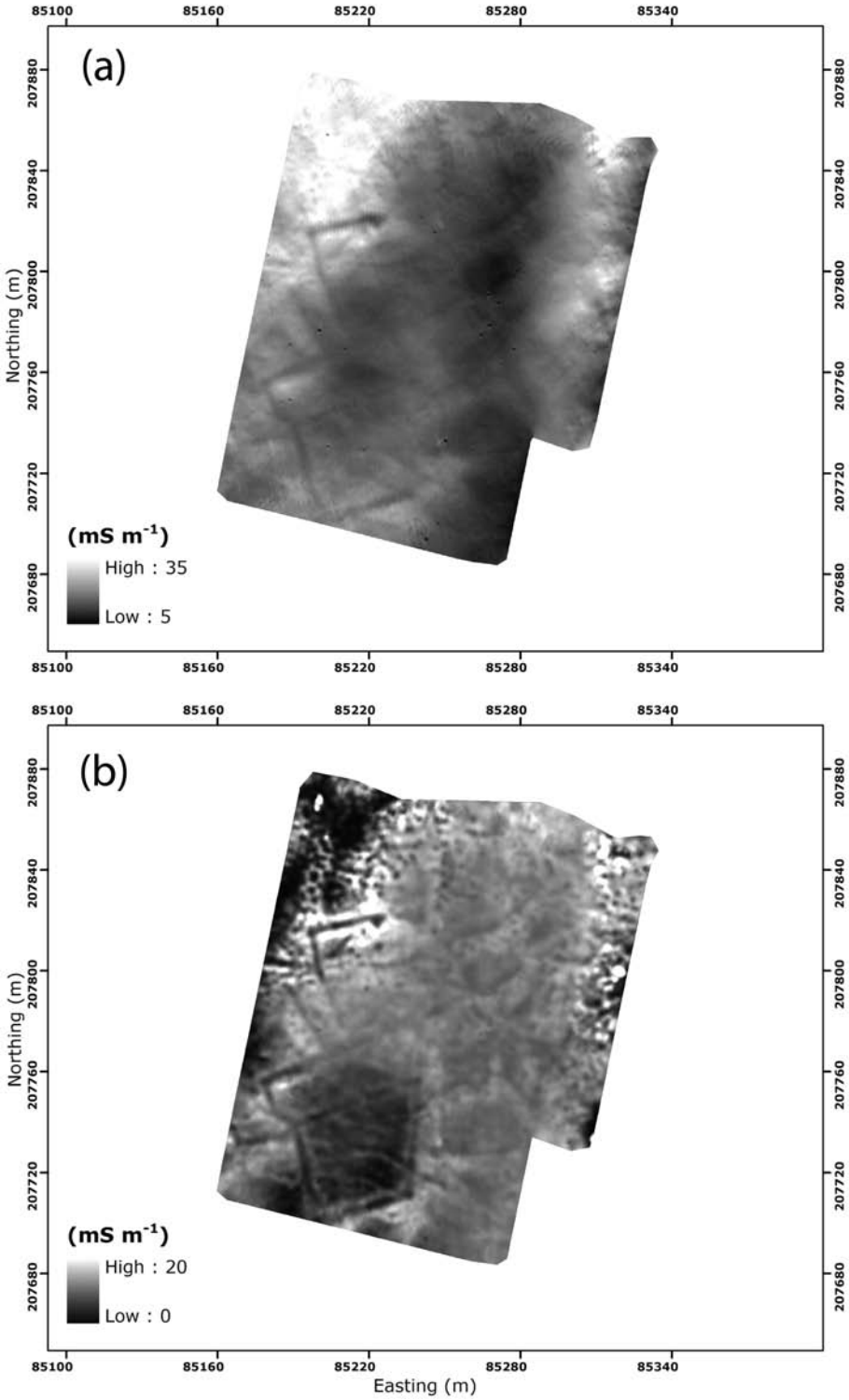

Fig. 5. ECa measured with the (a) PRP,1.1 coil configuration and (b) modeled EC^{*}_{sand}.

CONCLUSIONS

In this study, we showed how small soil anomalies could be better discerned by using a two-step inversion procedure on ECa data. By taking the large-scale variation of deeper soil layers, accurately described through EC-depth modeling, into account in the inversion procedure, the masking effect of these layers on less contrasting features was removed. This facilitated the identification of both anthropogenic and natural small-scale features (such as ditches and ice-wedge casts) in the upper soil layers.

We conclude that the integrated processing and coupled inversion of multiple simultaneous ECa measurements provides better perspectives to identify soil patterns at different spatial scales.

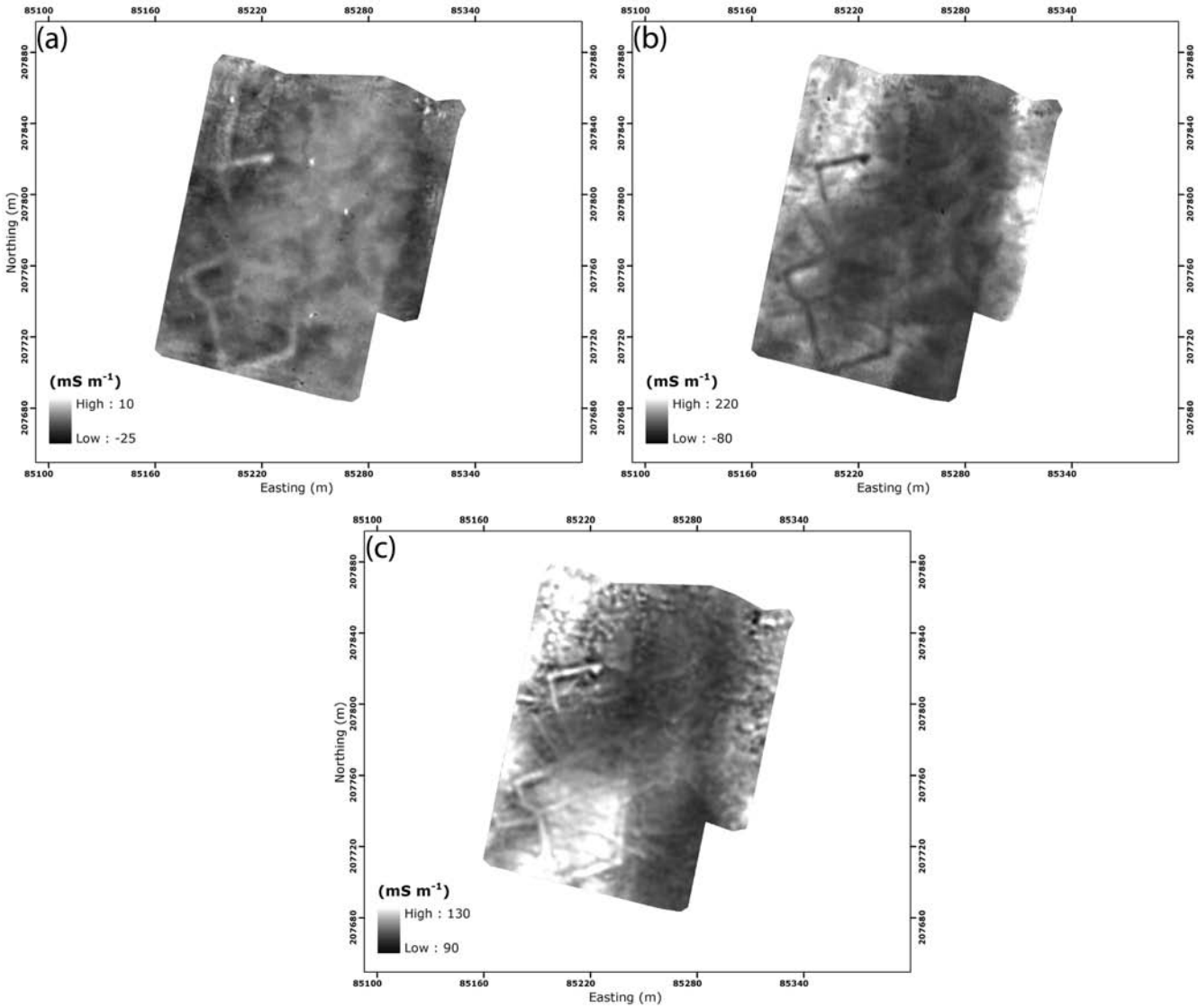

Fig. 6. (a) Modeled EC_1^* between 0 and 0.5 m, (b) EC_2^* between 0.5 and 1.0 m, and (c) EC_3^* deeper than 1.0 m.

ACKNOWLEDGMENTS

The authors would like to thank Valentijn Van Parys for his assistance with the field work and the farmers Gabriel and Filip Landuyt for granting us access to their field.

REFERENCES

Ameryckx, J., editor. 1962. Bodemkaart van Belgie, Verklarende tekst bij het kaartblad Maldegem 24W. Centrum voor Bodemkartering, Gent, Belgium.

Beamish, D. 2011. Low induction number, ground conductivity meters: A correction procedure in the absence of magnetic effects. J. Appl. Geophys. 75:244–253. doi:10.1016/j.jappgeo.2011.07.005

Borchers, B., T. Uram, and J.M.H. Hendrickx. 1997. Tikhonov regularization of electrical conductivity depth profiles in field soils. Soil Sci. Soc. Am. J. 61:1004–1009. doi:10.2136/sssaj1997.03615995006100040002x

Brevik, E.C., T.E. Fenton, and A. Lazari. 2006. Soil electrical conductivity as a function of soil water content and implications for soil mapping. Precis. Agric. 7:393–404. doi:10.1007/s11119-006-9021-x

Callegary, J.B., T.P.A. Ferré, and R.W. Groom. 2007. Vertical spatial sensitivity and exploration depth of low-induction-number electromagnetic-induction instruments. Vadose Zone J. 6:158–167. doi:10.2136/vzj2006.0120

Carroll, Z.L., and M.A. Oliver. 2005. Exploring the spatial relations between soil physical properties and apparent electrical conductivity. Geoderma 128:354–374. doi:10.1016/j.geoderma.2005.03.008

Cook, P.G., and G.R. Walker. 1992. Depth profiles of electrical conductivity from linear combinations of electromagnetic induction measurements. Soil Sci. Soc. Am. J. 56:1015–1022. doi:10.2136/sssaj1992.03615995005600040003x

Corwin, D.L., and J.D. Rhoades. 1982. An improved technique for determining soil electrical conductivity-depth relations from above-ground electromagnetic measurements. Soil Sci. Soc. Am. J. 46:517–520. doi:10.2136/sssaj1982.03615995004600030014x

De Clercq, W., P. De Smedt, J. De Reu, D. Herremans, P. Masters, T. Saey, B. Stichelbaut, and M. Van Meirvenne. 2012. Towards an integrated methodology for assessing rural settlement landscapes in the Belgian lowlands. Archaeol. Prospect. 19:141–145. doi:10.1002/arp.1418

Doolittle, J.A., K.A. Sudduth, N.R. Kitchen, and S.J. Indorante. 1994. Estimating depth to clays using electromagnetic induction methods. J. Soil Water Conserv. 49:572–575.

Fröhlich Gugler, A.I.M., and P. Gex. 1996. Electromagnetic survey of a Celtic tumulus. J. Appl. Geophys. 35:15–25. doi:10.1016/0926-9851(96)00024-9

Heilig, J., J. Kempenich, J. Doolittle, E.C. Brevik, and M. Ulmer. 2011. Evaluation of electromagnetic induction to characterize and map sodium-affected soils in the northern Great Plains. Soil Surv. Horiz. 52:77–88.

Hendrickx, J.M.H., B. Borchers, D.L. Corwin, S.M. Lesch, A.C. Hilgendorf, and J. Schlue. 2002. Inversion of soil conductivity profiles from electromagnetic induction measurements. Soil Sci. Soc. Am. J. 66:673–685. doi:10.2136/sssaj2002.0673

Inman, D.J., R.S. Freeland, J.T. Ammons, and R.E. Yoder. 2002. Soil investigations

using electromagnetic induction and ground-penetrating radar in southwest Tennessee. Soil Sci. Soc. Am. J. 66:206–211. doi:10.2136/sssaj2002.0206

Lück, E., J. Callmer, and T. Skanberg. 2003. The house of the Bailiff of Sövestad, Sweden– a multi-method geophysical case-study. Archaeol. Prospect. 10:143–151. doi:10.1002/arp.210

Marquardt, D. 1963. An algorithm for least-squares estimation of nonlinear parameters. SIAM J. Appl. Math. 11:431–441. doi:10.1137/0111030

McCutcheon, M.C., H.J. Farahani, J.D. Stednick, G.W. Buchleiter, and T.R. Green. 2006. Effect of soil water on apparent soil electrical conductivity and texture relationships in a dryland field. Biosystems Eng. 94:19–32. doi:10.1016/j.biosystemseng.2006.01.002

McNeill, J.D. 1980. Electromagnetic terrain conductivity measurement at low induction numbers. Technical Note TN-6. Geonics Limited, Missisauga, Ontario, Canada.

Meerschman, E., M. Van Meirvenne, P. De Smedt, T. Saey, M.M. Islam, F. Meeuws, E. Van De Vijver, and G. Ghysels. 2011. Imaging a polygonal network of ice-wedge casts with an electromagnetic induction. Soil Sci. Soc. Am. J. 75:1–6. doi:10.2136/sssaj2009.0216

Mester, A., J. van der Kruk, E. Zimmermann, and H. Vereecken. 2011. Quantitative two-layer conductivity inversion of multi-configuration electromagnetic induction measurements. Vadose Zone J. 10:1319–1330. doi:10.2136/vzj2011.0035

Minasny, B., and A.B. McBratney. 2006. A conditioned Latin hypercube method for sampling in the presence of ancillary information. Comput. Geosci. 32:1378–1388. doi:10.1016/j.cageo.2005.12.009

Monteiro Santos, F.A., J. Triantafilis, K.E. Bruzgulis, and J.A.E. Roe. 2010. Inversion of multiconfiguration electromagnetic (DUALEM-421) profiling data using a one-dimensional laterally constrained algorithm. Vadose Zone J. 9:117–125. doi:10.2136/vzj2009.0088

Persson, K., and B. Olofsson. 2004. Inside a mount: Applied geophysics in archaeological prospecting at the Kings' Mounds, Gamla Uppsala, Sweden. J. Archaeol. Sci. 31:551–562. doi:10.1016/j.jas.2003.10.003

Rhoades, J.D., and D.L. Corwin. 1981. Determining soil electrical conductivity-depth relations using an inductive electromagnetic soil conductivity meter. Soil Sci. Soc. Am. J. 45:255–260. doi:10.2136/sssaj1981.03615995004500020006x

Rhoades, J.D., S.M. Lesch, P.J. Shouse, and W.J. Alves. 1989. New calibrations for determining soil electrical conductivity—Depth relations from electromagnetic measurements. Soil Sci. Soc. Am. J. 53:74–79. doi:10.2136/sssaj1989.03615995005300010014x

Robinson, D.A., H. Abdu, I. Lebron, and S.B. Jones. 2012. Imaging of hill-slope soil moisture wetting patterns in a semi-arid oak savanna catchment using time-lapse electromagnetic induction. J. Hydrol. (Amsterdam) 416–417:39–49. doi:10.1016/j.jhydrol.2011.11.034

Saey, T., P. De Smedt, E. Meerschman, M.M. Islam, F. Meeuws, E. Van De Vijver, A. Lehouck, and M. Van Meirvenne. 2012a. Electrical conductivity depth modeling with a multireceiver EMI sensor for prospecting archaeological features. Archaeol. Prospect. 19:21–30. doi:10.1002/arp.425

Saey, T., M.M. Islam, P. De Smedt, E. Meerschman, F. Meeuws, E. Van De Vijver, A. Lehouck, and M. Van Meirvenne. 2012b. Using a multi-receiver survey of apparent electrical conductivity to reconstruct a Holocene tidal channel in a polder area. Catena 95:104–111. doi:10.1016/j.catena.2012.02.001

Saey, T., D. Simpson, H. Vermeersch, L. Cockx, and M. Van Meirvenne. 2009a. Comparing the EM38DD and DUALEM-21S sensors for depth-to-clay mapping. Soil Sci. Soc. Am. J. 73:7–12. doi:10.2136/sssaj2008.0079

Saey, T., D. Simpson, U. Vitharana, H. Vermeersch, J. Vermang, and M. Van Meirvenne. 2008. Reconstructing the paleotopography beneath the loess cover with the aid of an electromagnetic induction sensor. Catena 74:58–64. doi:10.1016/j.catena.2008.03.007

Saey, T., M. Van Meirvenne, H. Vermeersch, N. Ameloot, and L. Cockx. 2009b. A pedotransfer function to evaluate the soil profile textural heterogeneity using proximally sensed apparent electrical conductivity. Geoderma 150:389–395. doi:10.1016/j.geoderma.2009.02.024

Santos, V.R.N., J.L. Porsani, C.A. Mendonça, S.L. Rodrigues, and P.D. DeBlasis. 2009. Reduction of topography effect in inductive electromagnetic profiles: Application on coastal *sambaqui* (shell mound) archaeological site in Santa Catarina state, Brazil. J. Archaeol. Sci. 36:2089–2095. doi:10.1016/j.jas.2009.05.014

Slavich, P.G. 1990. Determining ECa-depth profiles from electromagnetic induction measurements. Aust. J. Soil Res. 28:443–452. doi:10.1071/SR9900443

Tromp-van Meerveld, H.J., and J.J. McDonnell. 2009. Assessment of multi-frequency electromagnetic induction for determining soil moisture patterns at the hillslope scale. J. Hydrol. 368:56–67. doi:10.1016/j.jhydrol.2009.01.037

Venter, M.L., V.D. Thompson, M.D. Reynolds, and J.C. Waggoner, Jr. 2006. Integrating shallow geophysical survey: Archeological investigations at Totógal in the Sierra de los Tuxtlas, Veracruz, México. J. Archaeol. Sci. 33:767–777. doi:10.1016/j.jas.2005.10.008

Vitharana, U.W.A., T. Saey, L. Cockx, D. Simpson, H. Vermeersch, and M. Van Meirvenne. 2008. Upgrading a 1/20,000 soil map with an apparent electrical conductivity survey. Geoderma 148:107–112. doi:10.1016/j.geoderma.2008.09.013

Wait, J.R. 1962. A note on the electromagnetic response of a stratified earth. Geophysics 27:382–385. doi:10.1190/1.1439028